Microstructure and bending properties of die-casting alloys at various chromium contents

E. Zanini, S. Barison, L. Capra, G. Timelli, F. Voltazza

A study of the effects of chromium addition on AlSi9Cu3(Fe) alloy was carried out. Die cast EN AC-46000 alloy plates for microstructural investigation and bend testing were produced using a multispecimen die in a high pressure, cold chamber machine. The Cr ranged within the tolerance limits of the EN AC-46000 type alloys, according to the EN 1706 standard. The investigations allowed evaluation of modifications to microstructural and bending properties produced by Cr additions. In particular, the microstructural analysis revealed that the morphology of primary sludge compounds was mainly cubic-type, such as polyhedral, star-like and blocky, while proeutectic α-$Al_x(Fe,Mn,Cr)_ySi_z$ intermetallics showed blocky or polyhedral morphology at any Cr level. Increasing the Cr content, the whole area fraction of these particles increased and the primary intermetallic compounds segregated in the central region of the cross section of the castings. This was associated to a mechanism similar to that suggested for the ESCs entrapment. The increase of brittle Fe-rich particles affected the fracture load and the displacement to fracture of the alloy at the highest Cr level.

Keywords: Aluminium alloys; Chromium; Microstructure; Casting defects; Mechanical properties; High-pressure die-casting

INTRODUCTION

Recycling of aluminium brings potential energy savings of up to 95% and produces 99% less emission than primary aluminium production from ore. The metal can also be recycled indefinitely, as reprocessing does not damage its structure [1]. Therefore, secondary aluminium and alloys are getting wide acceptance world-wide. The efficiency of aluminium recycling translates into high recycling rates for various applications. The lightness of aluminium alloy products contributes to fuel savings and reductions in emissions. Recycling rates for transport applications range from 60-90% in various countries [2,3]. In these terms, the aluminium industry is working with the automobile manufacturers to enable easier dismantling of aluminium components from cars in order to improve the sorting and recovery of aluminium. During recycling, most of the parts are mixed together regardless of their chemical composition, as sorting of the parts may not be commercially viable. Efforts are then made to correct the composition of the resulting alloy on line. This practice has economic limitations too. Furthermore, certain elements are

Enrico Zanini, Giulio Timelli*
University of Padova,
Department of Management and Engineering - DTG,
Stradella S. Nicola, 3 I-36100 Vicenza, Italy.
(*Corresponding author: Tel.: 00 39 0444 998769; fax. 00 39 0444 998889. E-mail address: timelli@gest.unipd.it (G. Timelli).

Silvio Barison, Filippo Voltazza
Toolcast S.n.c., Via Marconi 29, I-35020 Brugine (PD), Italy.

Leonardo Capra
Raffineria Metalli Capra S.p.A.,
Via Quinzano 96, I-25030 Castel Mella (BS), Italy.

Memoria vincitrice del premio Aldo Daccò 2011

either difficult and expensive to remove, such as iron [4].

Iron is always present in commercial Al-Si foundry alloys and has consistently emerged as the main impurity element and perhaps the most detrimental to the mechanical properties of these alloys.

It has been shown that the size and amount of iron-containing phases is strongly influenced by solidification rate [5-7] and that alloying elements such as Mn, Cr, Ni, Co, Sr, Mo, K and Be can change the morphology of the intermetallic phases or enhance the precipitation of phases which are less harmful than β-Al_5FeSi, i.e. a Chinese script or polyhedral morphology [5-15]. Manganese is the most common alloying addition, but it has been shown that Chromium has similar effect [7,12,16-18]. While manganese and/or chromium cause a beneficial change to the morphology of Fe-rich phases, it is that change in combination with large concentrations of Fe, Mn and Cr that leads to sludge formation in traditional secondary die casting alloys [19-21]. Due to high specific gravity, sludge compounds can settle to the floor of the furnace or crucible, thus reducing the furnace capacity, and change the chemical composition of the molten metal. Further, entrapment of the sludge into the mould cavity has a negative influence on the mechanical properties of castings [22].

Sludge formation has been shown to be time and temperature dependent process in a combination with the alloy's chemistry. A sludge factor (*SF*) has been suggested by Jorstad [23] and Gobrecht [24] for Al-Si-Cu alloys to act as a guide to avoid sludge formation. This factor is calculated from the formula:

$$\text{Sludge Factor } (SF) = (1 \times \text{wt.\%Fe}) + (2 \times \text{wt.\%Mn}) + (3 \times \text{wt.\%Cr}) \tag{1}$$

where Cr is the most deleterious element for the formation of sludge. Further, inconsistency exists in the sludge factor formula. Although the previous relationship is widely accepted,

Alloy	Fe	Cr	Si	Mg	Mn	Cu	Zn	Ni	Al	SF	SF´
1	0.780	0.057	9.210	0.220	0.180	2.996	1.213	0.074	bal.	1.31	1.16
2	0.770	0.087	9.055	0.220	0.200	2.940	1.194	0.072	bal.	1.43	1.24
3	0.740	0.119	9.120	0.230	0.200	2.950	1.199	0.073	bal.	1.50	1.28
4	0.740	0.153	9.050	0.230	0.210	2.960	1.201	0.097	bal.	1.62	1.36

TAB. 1   *Chemical compositions of the experimental alloys (wt.%). The sludge factors SF and SF´, obtained according to eqs. (1) and (2), are also shown for each alloy.*

Composizione chimica delle leghe utilizzate (%pond.). Per ogni lega vengono inoltre riportati i fattori di sludge SF e SF´, ottenuti tramite le eq. (1) e (2).

some prefer the relation [18]:

$$Sludge\ Factor\ (SF') = (1 \times wt.\%Fe) + (1,5 \times wt.\%Mn) + (2 \times wt.\%Cr) \quad (2)$$

Jorstad [23] and Gobrecht [24] showed that there exists a critical melt superheat temperature for AlSi9Cu3(Fe) type alloys above which the formation of sludge can be avoided. The problem of sludge formation occurs most often in the pressure diecasting industry where, in order to preserve the die, the melt holding temperature is typical lower than the other foundry processes. Therefore, aluminium alloys with the lowest Cr content of the composition tolerance limits are requested to secondary aluminium alloys producers. As the use of secondary aluminium alloys becomes more common, sludge is a problem of increasing importance due to the increasing concentration of Fe, Mn and Cr in the scrap cycle [1-4].

In this study, the influence of Cr content on microstructure and bending properties of secondary AlSi9Cu3(Fe) die casting alloy was investigated.

EXPERIMENTAL PROCEDURE
### Alloy and diecasting parameters
In the present work a secondary AlSi9Cu3(Fe) cast alloy (EN AC-46000, equivalent to the US designation A380) was supplied by Raffineria Metalli Capra as commercial ingots and used as a base-line. The ingots were melted in a 300 kg SiC crucible in a gas-fired furnace set up at 800 ± 10°C and maintained at this temperature for at least 3 hours. The temperature of the melt was then gradually decreased by following the furnace inertia up to 690 ± 5°C. The molten metal was then degassed with an argon–sulphur hexafluoride mixture (Ar/SF$_6$ 0.2%) and periodically was manually skimmed and stirred with a coated paddle to avoid any type of sedimentation. The furnace temperature is the holding temperature commonly used for EN AC-46000 type alloys, which is enough to avoid sludge formation [23,24]. Trace additions of Cr were made to the melt in the form of commercial Al-20Cr master alloy, which was added to the molten metal as waffle ingots. Four alloys were prepared with Cr content ranging from 0.057 to 0.153 wt.% according to the composition tolerance limits of the EN 1706:2010 standard. The chemical composition, measured on separately poured samples, did not change within every set of analysed alloy and it is shown in Table 1.

Casting was carried out on an Italpresse 2.9 MN locking force cold chamber HPDC machine. The machine was equipped with a dynamic shot control system so that the plunger velocity, pressure, and time could be continuously monitored and recorded during the process. Thus, each casting was documented with its shot profile, to monitor the final quality and repeatability. A multicavity die, with geometry shown in Figure 1, was used to produce high-pressure diecast specimens. The weight of the

aluminium alloy diecasting was 0.9 kg, including the runners, gating and overflow system.

The first 20 to 25 castings were discarded after the start-up to reach a quasi-steady-state temperature in the shot chamber and die, and ensure specimen consistency. The die temperature was maintained at ~230°C by circulating oil through channels in the die. The melt was transferred from the holding furnace and poured into the shot sleeve by means of a cast iron ladle coated with an insulated paste. The temperature measurement during the melt transfer from the casting furnace to the shot sleeve evidenced a continuous dissipation of the melt superheat, ~50°C, at an average cooling rate of ~2.7°C/s [22]. The fill fraction of the shot chamber, with a 70 mm inner diameter, was kept at 0.28. The plunger velocity was 0.2 ms^{-1} for the first phase and 2.7 ms^{-1} for the filling phase; an intensification pressure (IP) of 40 MPa was applied once the die cavity was full to guarantee high-integrity die castings.

This study only examined rectangular plates for bending eva-
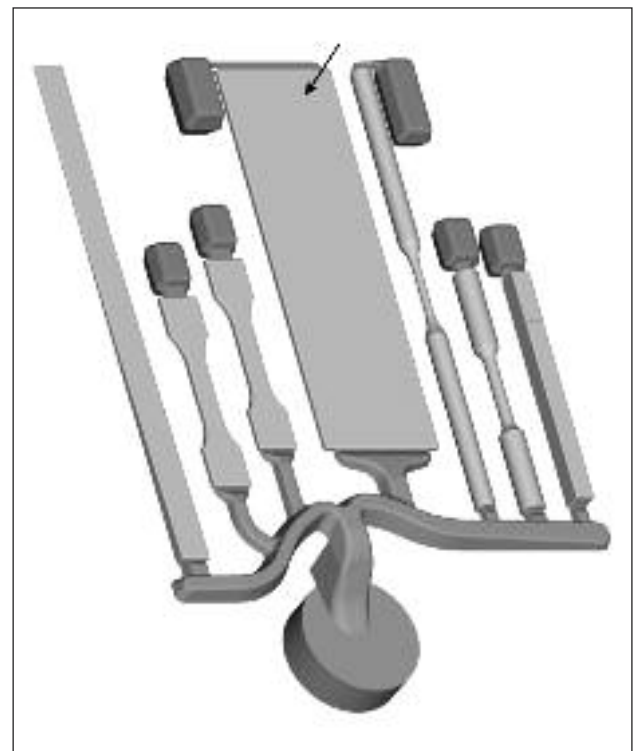
FIG. 1   *Geometry of multicavity die used in this study. Investigated plate is from the position indicated by arrow.*

Geometria del getto multi-impronta per la realizzazione di provette per test meccanici. Viene indicata la piastra oggetto di studio.
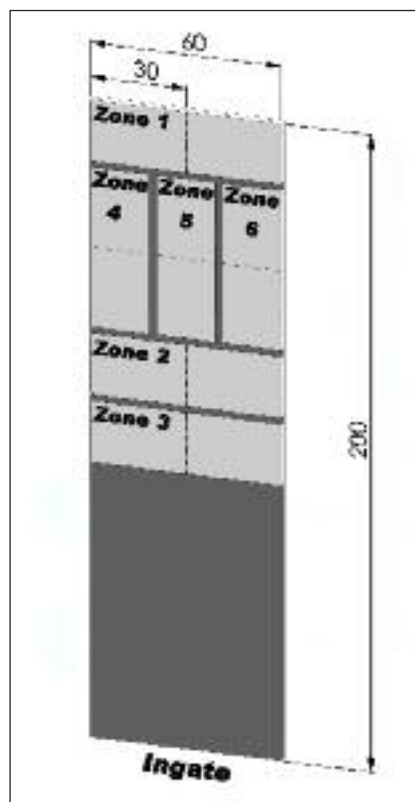
FIG. 2
Illustration of the diecast plate showing the investigated locations.

Illustrazione della piastra pressocolata dove si mostrano le posizioni indagate.

luation indicated in Figure 1. In order to assure an acceptable level of soundness before mechanical testing and to localise the porosity distribution, the plates were analysed by means of a Bosello SRE 80 industrial machine equipped with a microfocus X-ray set up at 70 kV and 80 μA.

Bending test
To elucidate the effects of a different Cr content, the plates were machined into three point bend specimens as shown in Figure 2. Some specimens were machined as aligned with the principal flow direction of the metal during die filling, while others were drawn 90° to the flow direction. The bending specimens drawn from the zones 1, 2 and 3 were 19.2 mm wide, had a length of 60 mm and a thickness of 3 mm; while the specimens from the
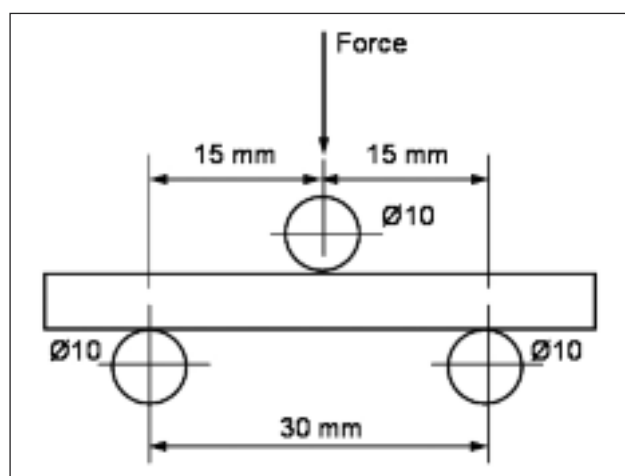
FIG. 3   **Sketch of three point bend test adopted in this work.**

Schema del test di flessione a tre punti utilizzato nel presente lavoro.

zones 4, 5 and 6 had dimensions $17.7 \times 50 \times 3$ mm^3, respectively. The as-diecast specimens has been stored at room temperature for about seven months before being tested and were therefore similar to a T1-condition.

By subjecting the specimens to three point bending tests, the surface material experiences larger strains and stresses compared to the interior material. It is therefore expected that the fracture initiates in the surface layer during these tests, even when the surface material is more ductile than the interior material. The three point bend test was employed as shown in Figure 3 by using an MTS 810 Material Test System machine with a load applied to the centreline, according to the standard ASTM E290-09. The crosshead speed used was 1 mm/min. The fracture occurs at maximum force. Experimental data were collected and processed to provide fracture load (P_f) and displacement to fracture (W_f). Seven or more plates were tested for each alloy.

Metallography and image analysis
Different bend specimens, from those mechanical tested, were selected for metallographic investigations. The samples cut from the cross section of the length were mechanically prepared to a 3-μm finish with diamond paste and, finally, polished with a commercial fine silica slurry. Microstructural analysis was carried out using an optical microscope and a scanning electron microscope (SEM) equipped with an energy-dispersive spectrometer (EDS), and quantitatively analyzed using an image analyser. Various microstructural parameters were investigated and measured, such as the particle average size (μm), aspect ratio, area fraction and distribution of Fe-bearing compounds. Size is defined as the equivalent circle diameter (d), while the aspect ratio (α) is the ratio of the maximum to the minimum Ferets.

To obtain a statistical average of the distribution, a series of at least 15 photographs of each specimen were taken. The secondary phases, such as the Mg_2Si and $CuAl_2$ particles, were excluded from the measurements. The polished specimens were also etched in a modified Murakami etchant (60 mL H_2O, 10 g NaOH, and 5 g $K_3Fe(CN)_6$) so that, at low magnification, the α-Al phase and the Al-Si eutectic and intermetallics appeared white and black, respectively, and, therefore, easily distinguishable.

Numerical simulation of the HPDC process
The MAGMASOFT® v.4.2. (2002) software [25], with its module for high-pressure die casting MAGMAhpdc, was used for numerically simulating the filling behaviour of the analysed plate. Basic governing equations of MAGMASOFT® are continuity equation, Navier–Stoke's equation, energy equation and volume of fluid (VoF) method for the free surface movement during the die filling. MAGMAhpdc employs the finite volume approach to convert differential equations into algebraic ones and solve them on a rectangular grid. A three-dimensional (3-D) simulation model was created and it was automatically meshed by the software with about 280000 cells for the plate cavity. The edge length of the smallest element was chosen to be 0.1 mm so as to ensure at least thirty layers of elements in the thin wall section of the plate.

The physical constants and properties of the die and the alloy, and their evolution with temperature, were chosen among those present in the software database, as well as the heat transfer coefficients (HTC). The temperature of the die for the first cycle was assumed to be at a uniform temperature of 230°C, while, for the subsequent cycles, the initial temperature in the die is taken to be the predicted temperature distribution at the end of the previous cycle. A number of 10 numerical cycles were taken after the start up to reach a quasi-steady state temperature in the die. To define the whole set of boundary conditions in the

model, the process parameters (e.g. regarding the filling and cooling cycle) and the cycle time, acquired from the casting process, were imported in the software, increasing the reliability of numerical simulation.

RESULTS AND DISCUSSION
### General observations

Typical macrostructures taken across the thickness of diecast samples are shown in Figure 4 and they are almost similar in all the analysed specimens, independently of Cr level. The primary α-Al crystals appear with light grey tone, while the Al-Si eutectic appears darker. Some Fe-bearing intermetallic particles are present with darker or approximately similar grey-tone as the eutectic. Dark bands of positive segregation, commonly called defect bands, follow the contour of the casting surface. This is a typical microstructural feature observed in Al-Si die castings [26-28]. Defect bands were observed at all Cr levels investigated and no significant concentrated porosity was observed in the defect bands. In recent years defect bands have received significantly attention [29]. A premise for their formation in solidifying high-pressure die-cast alloys is the presence of localized deformation within a mushy zone adjacent to the die wall, when the alloy behaves as a granular material. Partially solid microstructures deform as cohesionless granular materials during processing, due to a combination of their small grain size (~10 μm), relatively unbranched equiaxed crystal shape, and the significant shear stresses (≤100 MPa) that act during HPDC. This behaviour leads to increase the volume of interparticle spaces, producing dilatant bands in which the solid packing density is lower than the adjacent material [29]. In aluminium die casting alloys, these bands contain a higher liquid fraction and, therefore, a higher solute content (positive macrosegregation) than their surroundings. Defect bands generally form during the die-filling stage and during the pressurization stage [26], and their position and appearance are affected by changes in casting conditions, and depend on the alloy composition [26,30].

Different forms of positive macrosegregation were found in the analysed alloys. The macrosegregation profiles consist on the whole of three components. The first is a general increase in the eutectic fraction from the casting centre to the surface. The second component of the macrosegregation profile is a surface macrosegregation. For the samples in this study, this surface layer has no clear boundary, but its thickness, ~30 to 50 μm, is significantly smaller than that of other defect bands. It was proposed that this positive macrosegregation results from a combination of inverse segregation and exudation [30]. The third component is the aforementioned positive macrosegregation localised in a narrow region, ~60 μm thick, at about 250 ± 15 μm below the casting surface (Figure 4). These bands could have formed during the die filling stage [27,28].

Inner defects bands, whose formation is generally associated to the pressurization stage during HPDC process, were not revealed in the present work, contrary to what observed in Ref. [22,32]. According to Otarawanna et al. [31], the feeding mechanism and the inner defect bands formation depend on the combination of the IP applied and the gate thickness. When a sufficiently high IP and thick gate are used, defect banding occurs through the gate and appears to play a key role in tran-

FIG. 4
Typical AlSi9Cu3(Fe) (0.057 wt.% Cr) macrostructures across the thickness of the diecast plate in T1-condition showing defect bands, and area fraction and distribution of ESCs. The macrographs refer to the regions (a) near the overflow and (b) near the gate. Darker material in the macrograph contains a higher fraction of eutectic, while ESCs are large light grey crystals.
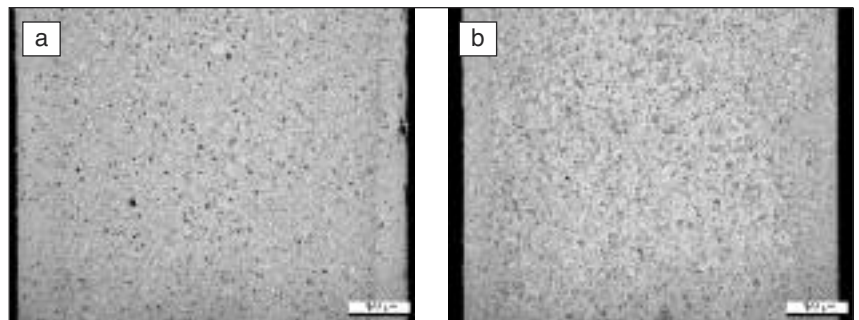
Tipiche macrostrutture della lega AlSi9Cu3(Fe) (0.057 %pond Cr) ottenute da sezioni trasversali delle piastre allo stato T1; si evidenzia la presenza di bande di segregazione e la distribuzione degli ESCs. Le macrografie si riferiscono alle regioni (a) vicino al pozzetto e (b) in prossimità dell'attacco di colata. Le zone che appaiono più scure nella macrografia indicano la presenza una frazione eutettica più elevata, mentre gli ESC si presentano come grossi cristalli chiari.
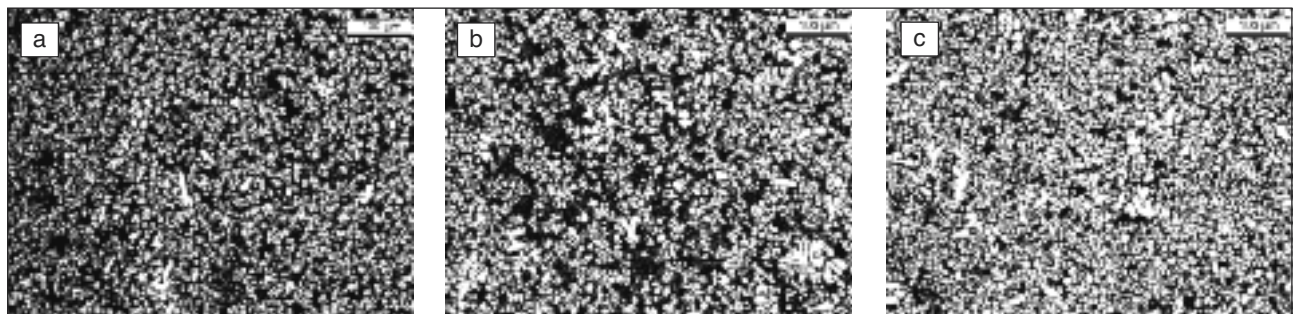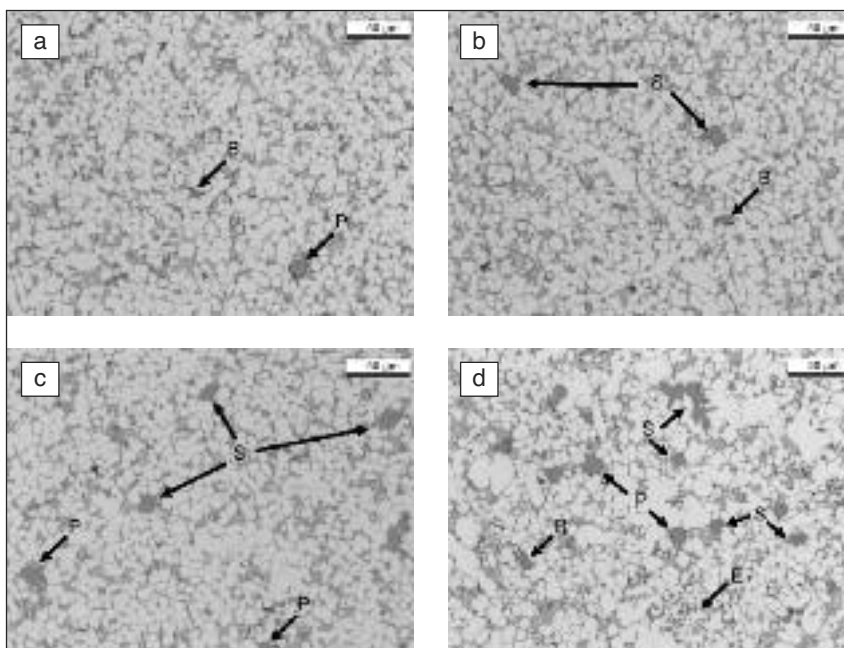

Fig. 5 *Etched microstructures obtained from different positions across the thickness of AlSi9Cu3(Fe) (0.057 wt.% Cr) diecast plates in T1-condition: (a) the casting surface, (b) within the defect band and (c) the centre of the casting. Primary -Al grains appear bright, whereas eutectic and secondary phases are dark.*

Microstrutture, dopo attacco chimico, ottenute da differenti posizioni delle piastre pressocolate in lega AlSi9Cu3(Fe) (0.057 %pond Cr) allo stato T1: (a) superficie del getto, (b) zona interna alle banda di segregazione e (c) centro della piastra. I cristalli primari di -Al appaiono chiari, mentre l'eutettico e le fasi secondarie sono scure.

FIG. 7
Typical microstructures of Cr-added AlSi9Cu3(Fe) alloys: (a) 0.057 wt.% Cr, (b) 0.087 wt.% Cr, (c) 0.119 wt.% Cr and (d) 0.153 wt.% Cr. Micrographs refer to the centre of the thickness of the diecast plates in T1-condition. B-Blocky, E-exploded, P-Polyhedral, S-Star-like particles.

Tipiche microstrutture delle leghe AlSi9Cu3(Fe) dopo alligazione al Cr: (a) 0.057, (b) 0.087, (c) 0.119 e (d) 0.153 %pond. Le micrografie si riferiscono al centro della sezione della piastra. Particelle B-Blocky, E-exploded, P-Polyhedral, S-Star-like.

sporting material into the casting in the latter stages of HPDC. When a low IP is combined with a thin gate, defect banding does not occur through the gate and feeding is less effective.

The typical microstructures obtained from different positions across the thickness of diecast samples are also shown in Figure 5. The micrographs refer to the casting surface, the region of the defect band and the centre of the castings, respectively.

Important factors affecting the distribution of the eutectic fraction and segregation phenomena are the presence and the amount of externally solidified crystals (ESCs) [28,29], which, mainly formed in the shot sleeve, are injected into the die cavity during die filling [33]. The ESCs are not equivalent to the cold flakes [34], which occasionally form due to the breaking up of the solid layer at the shot sleeve wall, but instead are single-crystal dendrites, as shown in Figure 6. ESCs with both branched-dendritic and globular-rosette morphology are present in the samples. In every plate, independently of Cr content, a higher fraction of ESCs was observed near the gate (~69%) and a lower amount, in the range between 5 and 9%, was observed further from the gate (Figure 4). This behaviour is explained considering the inhomogeneous temperature distribution in the shot sleeve which is inherently present in cold-chamber HPDC, and therefore resulting in non-uniform solidification conditions [35]. The metal far from the gate possesses a thermal history originating from the hotter shot chamber end and therefore contains few ESCs, while that closer to the gate originates from closer to the plunger and contains a larger fraction of ESCs. Additionally, a solidifying surface layer forms during filling of the die cavity and it constricts the metal to flow in the centreline of casting. Therefore, as observed in Figure 4, the ESCs are forced toward the casting centre.

Another factor to be considered for ESCs distribution and amount is the die temperature. Laukli et al. [36] underlined how the position of the ESCs can be influenced by the die temperature, because this affects the degree of metal-die flow constraint. Lower die temperature means similar flow constraint from all parts of the die wall, therefore the lift forces toward the centre of the cross section are symmetrical in the cross section, resulting in centred ESC distribution. Contrary, with increasing die temperature, the fluidity increases because less solidification occurs at the die walls and there is a decrease in the degree of

constraint to flow at the walls. This can induce a displaced ESC distribution or even a continuous flow of ESCs through the die toward the overflows.

Differences in solidification between wall and centre of sections reflect upon dimension and morphology of eutectic Si particles of the analysed alloys in T1-condition. Along the die wall, the nucleation prevails on growing mechanism due to an elevated undercooling; therefore, the formation of a fine and fibrous eutectic silicon is promoted. It is well established that rapid solidification changes the eutectic Si shape so that it is similar to chemically modified eutectic Si [37]. On the other hand, the eutectic Si particles shows a typical coarse plate-like morphology in the centre of plates, typical of unmodified aluminium alloys. Many eutectic Si particles are seen to lie along the Fe-bearing particles, suggesting Fe-rich intermetallics favour the formation
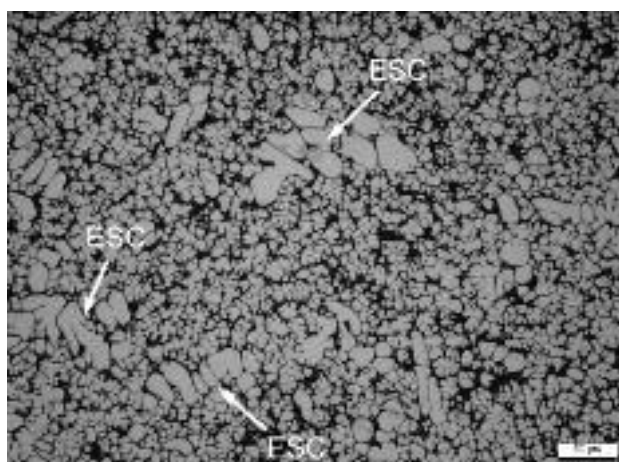
FIG. 6 ***Etched microstructure obtained at the centre of the thickness of diecast plates in T1-condition. ESCs are indicated with arrows. Primary α-Al grains appear bright, while Al-Si eutectic appears dark.***

Microstruttura, dopo attacco chimico, ottenuta al centro della sezione della piastra. Viene indicata la presenza degli ESCs. I cristalli primari di α-Al appaiono chiari, mentre l'eutettico Al-Si appare scuro.
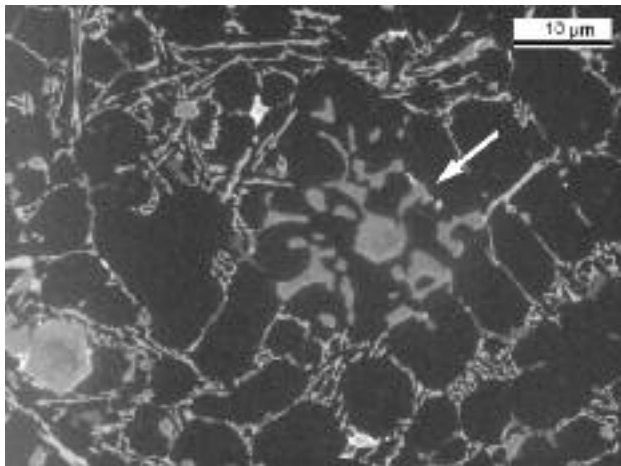
FIG. 8 *Exploded intermetallic compound in 0.153 wt.% Cr-added AlSi9Cu3(Fe) alloy.*

Fase intermetallica "esplosa" in una lega AlSi9Cu3(Fe) contenente lo 0.153 %pond di Cr.

of Si particles, and also that most of them precipitate in a pre-eutectic reaction.

Cu-bearing particles were also detected and characterized as θ-Al_2Cu intermetallics. Al_2Cu phase occurs in the form of both pockets of fine eutectic ($Al + Al_2Cu$) in the interdendritic regions and block-like Al_2Cu particles. The former is due to high cooling rate while the latter is consequence of high fraction of Fe-rich intermetallics, nucleating site for Al_2Cu and resulting from relatively low cooling rate.

Intermetallic compounds

Figure 7 shows the microstructures taken at the centre of the thickness of the plates diecast with different Cr content. Large blocky-like α-$Al_x(Fe,Mn,Cr)_ySi_z$ particles were observed in the microstructures. These phases or complex intermetallic compounds (Fe/Mn/Cr-containing phases) are usually called sludge, which may be primary in high Si content cast Al alloys. The sludge morphologies observed were mainly cubic-type form, such as polyhedral, star-like and blocky (Figure 7), instead of platelet/acicular form. Fe is tied up with trace elements, i.e. Mn and Cr, to form a new phase, which has an anisotropy in surface energy that gives rise to the observed morphologies, with the growing planes corresponding to the lowest surface energy. Therefore, the primary sludge crystals tend to be limited by the (111) faces and they appear as more or less well-formed hexagons [38]. Generally, a higher Mn content leads to more Chinese script morphology of Fe-rich phases, while higher Cr amount promotes the formation of polyhedral, star-like and blocky particles [19,20].

In the alloy 4, with the highest Cr content, sludge particles with an exploded shaped were also observed (Figure 7d). These intermetallics were generally found surrounded by primary α-Al phase. The convoluted arm structure occurs after the α-Al dendrites have begun to solidify, that is α-Al and α-$Al_x(Fe,Mn,Cr)_ySi_z$ form a coupled eutectic (Figure 8). The primary intermetallics, formed at high temperature, tie up with Si present in the alloy and consume it; this shifts the local chemical composition of the melt to the aluminium side of the phase diagram, resulting in a nucleation of α-Al primary phase around the intermetallics and in a coupled eutectic growing mechanism [20]. At lower cooling rates and higher chromium concentrations, the α-$Al_x(Fe,Mn,Cr)_ySi_z$ phase may form as a primary phase. In such conditions, it precipitates with the polyhedral morphology identified at the centre of the particle shown in Figure 8 and, as solidification progresses and the α-Al begins to form, the convoluted arm structure associated with the coupled eutectic growth.

Cooling rate also affects the morphology of sludge particles. Chinese script and β-needle Fe-rich compounds generally form at low cooling rates [19]. Therefore, the cooling rate during sludge

FIG. 9
(a) Backscattered SEM micrograph of coarse sludge compounds and (b) through (d) corresponding EDS composition maps.

(a) Micrografia BSE-SEM di grosse particelle di sludge e (b)-(d) mappatura EDS corrispondente.
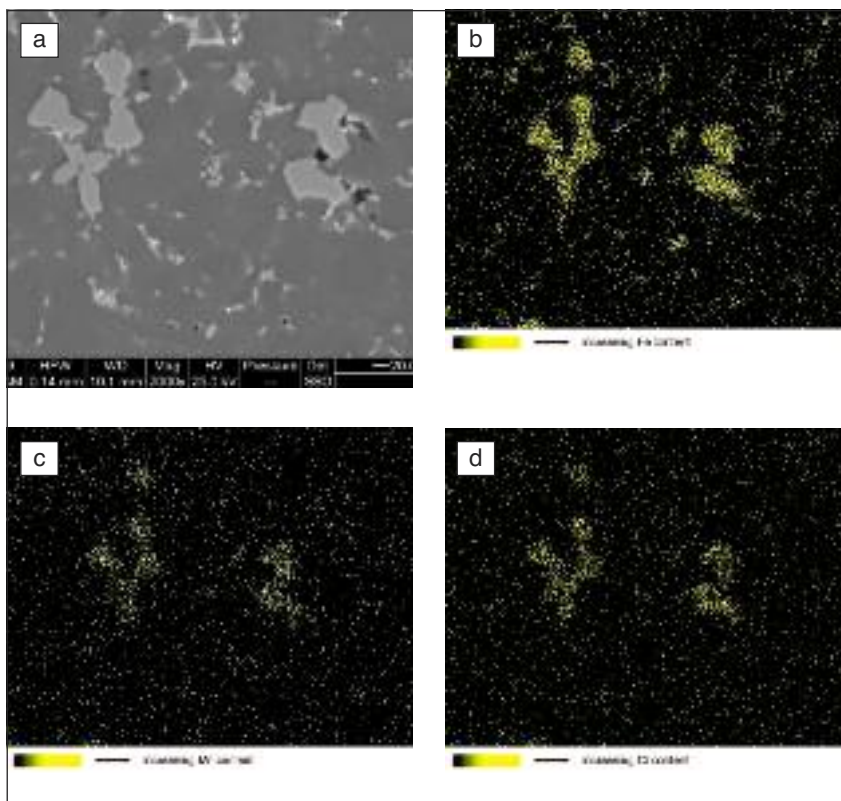
TAB. 2
Average area fractions of Fe-rich intermetallic particles in the investigated alloys. Sludge particles or overall Fe-bearing (primary and proeutectic) phases are considered. Particles with equivalent diameter higher than 3.6 μm were considered sludge. Standard deviation in parentheses.

Alloy	Cr level (wt.%)	Area fraction of sludge particles f' (%)	Area fraction of overall Fe-rich phases f (%)	f'/f
1	0.057	0.31 (0.1)	2.1 (0.6)	0.15
2	0.087	0.58 (0.15)	2.4 (0.8)	0.24
3	0.119	1.03 (0.2)	2.6 (0.5)	0.40
4	0.153	1.51 (0.17)	3.1 (1.2)	0.49

Frazione d'area delle particelle intermetalliche ricche in Fe nelle leghe analizzate. Vengono riportati i valori medi riferiti alle sole particelle di sludge e a quelle complessive (primarie e proeutettiche). Sono considerate come sludge le particelle con diametro equivalente maggiore di 3.6 μm. La deviazione standard tra parentesi.

formation is relatively high in the present work to prevent the formation of primary Chinese script and large needle-like particles.

The SEM-EDS mapping result in Figure 9 shows the relatively high Fe, Mn and Cr contents in the sludge compounds. Recently, Shabestari [20] and Warmuzeka et al. [39] showed how the stoichiometry and the crystal structure of the polyhedral, star-like and exploded sludge particles are the same, α(bcc) $[(Al_{12}(Fe,Mn,Cr)_3Si_i)]$.

Secondary fine α-$Al_x(Fe,Mn,Cr)_ySi_z$ particles, as revealed by the EDS analysis, were observed in all four alloys. These proeutectic intermetallic compounds, located at grain boundaries and predominantly in the interdendritic channels, do not contribute to the sludge. The proeutectic α-$Al_x(Fe,Mn,Cr)_ySi_z$ intermetallics show blocky or polyhedral morphology. The form depends upon the combination of Mn and Cr content and the undercooling degree. High cooling rate promotes nucleation of secondary α-phase, while β-phase formation results from low solidification rate [5,6]. Due to rapid solidification during HPDC and insufficient solute mixing, particle clustering of secondary α-$Al_x(Fe,Mn,Cr)_ySi_z$ particles were observed. Such distribution can alter the stress field in the vicinity of a cluster, giving rise locally to triaxial stresses much higher than the remote stress applied to the material. As a result, these particle segregations can act as crack or decohesion nucleation sites or both at remote stresses lower than the matrix yield strength, causing the material to fail at low-stress levels. A comparison of the chemical composition and crystal structure of the primary and proeutectic α-$Al_x(Fe,Mn,Cr)_ySi_z$ particles revealed that the latter phases contain more Mn or Cr than Fe, and show simple cubic structure [40].

Both the amount and the size of Fe-rich precipitates increased with Cr addition. This is because part of the Fe in the melt pre-

cipitates as polyhedral phase α prior to the eutectic and consequently the area fraction of these compounds increases. Table 2 shows the quantitative results of the average area fraction of sludge particles (f') and overall primary and proeutectic Fe-bearing phases (f) in the analysed alloys. Only particles with equivalent diameter higher than 3.6 μm were considered sludge. It is observed how the f'/f ratio increases by increasing the Cr level in the alloy, i.e. the sludge formation gradually prevails upon the overall Fe-rich precipitation under these process conditions. Recently, it was evidenced how the amount of sludge particles can be estimated from the sludge factor by a linear relationship [22]. Any increase in the area fraction of Fe-rich intermetallics is related to the size of the particles, which increase from ~1.9 μm at 0.057 wt.% Cr to ~2.8 μm at the highest Cr level. Contrary, the aspect ratio is steady in the range of 1.6 to 1.7. This evidences that an increasing Cr content, within the analysed range, in a secondary AlSi9Cu3(Fe) alloy with 0.75 wt% Fe and 0.20 wt.% Mn, does not change the morphology of Fe-bearing compounds, which present mainly a cubic-type shape.

The analysis of the size distribution of Fe-bearing phases was carried out for each alloy (Figure 10). It is observed how the particle size distribution varies according to the Cr level in the alloy. By increasing the Cr content in the base alloy, the size distribution of the compounds becomes more spread (Figure 10). The equivalent diameter of Fe-rich intermetallics with the maximum frequency shifts slightly to higher d values and the absolute value of the maximum frequency decreases. In particular, this behaviour is appreciated by increasing the Cr content up to 0.153 wt.%, where the microstructure is characterised by coarser α-$Al(Fe,Mn,Cr)Si$ particles; while, up to 0.119 wt.% Cr, the formation of a high number of fine α-phase particles is predominant. The size distributions of both primary and proeutectic Fe-rich intermetallics in the different alloys was investigated and found to follow the lognormal distribution. The probability density function of the three-parameters lognormal distribution can be written as:

$$f(d) = \frac{1}{(d-\tau)\sigma\sqrt{2\pi}}\exp\left[-\frac{(\ln(d-\tau)-\mu)^2}{2\sigma^2}\right] \quad (3)$$

where d is the equivalent diameter of intermetallic particles, τ the threshold, σ the shape and μ is the scale parameter [41]. The coefficient of the determination R^2 was used to evaluate the quality of the fitting. In the present work, the coefficient R^2 is 0.99, suggesting a good agreement of particle size distribution with the three-parameters lognormal distribution adopted.

Sludge distribution in diecast plates

In all the castings, the sludge particles tend to accumulate in the central region of the cross section of the plates, while there exists a surface layer with few primary sludge crystals (see Figure 4). Therefore, the casting plates contain a surface layer with randomly oriented fine grains of 4 to 10 μm [32] and few sludge compounds, and a central region containing a mixture of ESCs
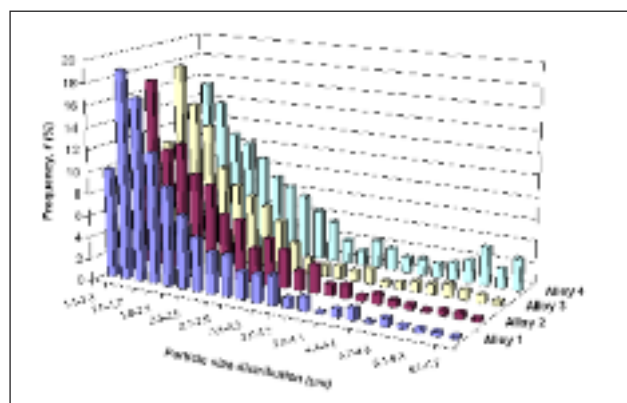
FIG. 10 *Distribution of Fe-bearing compounds both sludge and proeutectic particles.*

Distribuzione dei composti intermetallici primari e proeutettici ricchi in Fe.

of 50 to 100 μm, fine grains and sludge. Such HPDC microstructures are therefore characterised by a bimodal distribution of microstructural features [42]. This sludge-depleted layer appears as near-parallel lines in transverse sections over most of the length of the plate section in all the alloys.

Such segregation mechanism is similar to that suggested for the ESCs entrapment [36,43]. The high concentration of sludge particles, and ESCs, towards the centre of the casting is probably due to high shear developed near the die wall. Therefore, solid particles would migrate towards the region of highest velocity and lowest shear, following a quasi-Lagrangian model. At the same time, a surface skin rapidly grows during die filling altering the flow behaviour locally by reducing the effective cross section thickness and it exerts a pressure on the interior. Sludge particles, as well as ESCs, are not stationary ahead of the growth front, but they are carried in the liquid that flows parallel to the solidifying wall layer, impeding the natural entrapment. Furthermore, the surface layer is relatively fine compared with the size of sludge particles, making mechanical entrapment more difficult. Thus, a larger area fraction of sludge particles and ESCs are observed in the centre, without any segregation within the defect bands.

Sludge formation in cold-chamber HPDC

According to the Gobrecht [24], Jorstad [23] and Shabestari [20] relations, the holding temperature used in the present work is high enough so that sludge should not form in the furnace. However, the continuous dissipation of the melt superheat, mea-
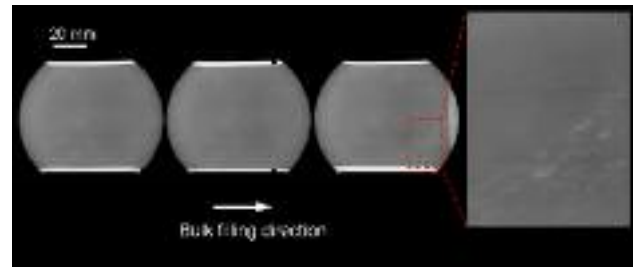
FIG. 11 *Micro-focus X-ray image of diecast plate showing the presence of macro porosity in the regions close to the overflows.*

Immagine ai raggi-X di una piastra pressocolata dove si evidenzia la presenza di macroporosità nelle regioni in prossimità del pozzetto.

sured during the melt transfer from the casting furnace to the shot sleeve, evidenced a drop of casting temperature. Therefore, with a reduced melt temperature a low temperature gradient and a large thermal undercooling are established adjacent to the shot sleeve wall in which externally solidified crystals, and eventually sludge particles, can form. Therefore, during the transport of molten metal from the casting furnace to the shot sleeve and inside the cold chamber, the sludge can be formed at the wall and eventually separate before the melt entered the die cavity. The wall crystals, with a polyhedral shape, are transported into the bulk of the liquid during filling by the flow of melt and survive as the melt is sufficiently cold.

Besides the Cr content, the cooling rate during sludge formation is relatively high to prevent the formation of coarse primary Chinese script and needle-like particles. In Al-Si-Cu alloys, Flores et al. [44] found that the sludge particles form most readily at about 640°C, reaching an average size of 40 μm after holding for just one to two minutes.

To demonstrate the importance of the heat loss by the molten metal, a simulation of temperature evolution in the melt during the shot sleeve filling evidenced a non-isothermal melt conditions in the shot sleeve with a ~10% solid fraction formed before the plunger's movement [45]. In the present work, this is indicative of the presence of both ESCs and sludge particles.

Radioscopic investigations

The preliminary X-ray analysis, carried out on each plate, revealed the presence of macro porosity on the regions close to the overflows where, due to the local die filling condition, air bubbles were entrapped and dragged (Figure 11). Air entrapment porosity is the most frequent defect found in HPDC products. Air bubbles form in turbulent liquid metal vein in different phases of the process and, consequently, they originates in different locations, but mostly inside the die cavity if air can not adequately flow away from the cavity. The air entrapment porosity is typically found far from its origin. The final distribution of cavities within the diecast product is related to the path followed by the molten metal.

The defect areas correspond to the zones named 1, 4 and 6 (see Figure 2). The reasons of this behaviour will be explained in the further section with the use of the numerical simulation of die filling.

Bending test

The bending properties such as the fracture load and displacement to fracture for all the alloys in the T1-condition are shown in Figure 12 as a function of the Cr content. The results are displayed according to the analysed regions, which should be grouped into two main sets according to the differences in the
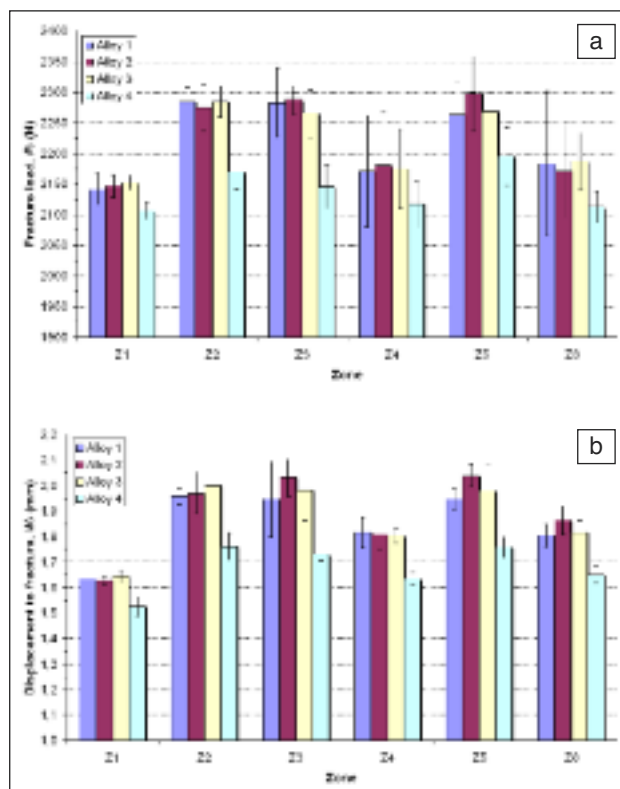
FIG. 12 *Average (a) fracture load and (b) displacement to fracture as a function of Cr content in AlSi9Cu3(Fe) alloy; the results are displayed according to the analysed regions of the plate. Standard deviations are given as error bars.*

Valori medi del (a) carico e (b) spostamento a rottura in funzione del livello di Cr; i risultati sono mostrati secondo le posizioni indagate nella piastra (deviazioni standard come barre d'errore).
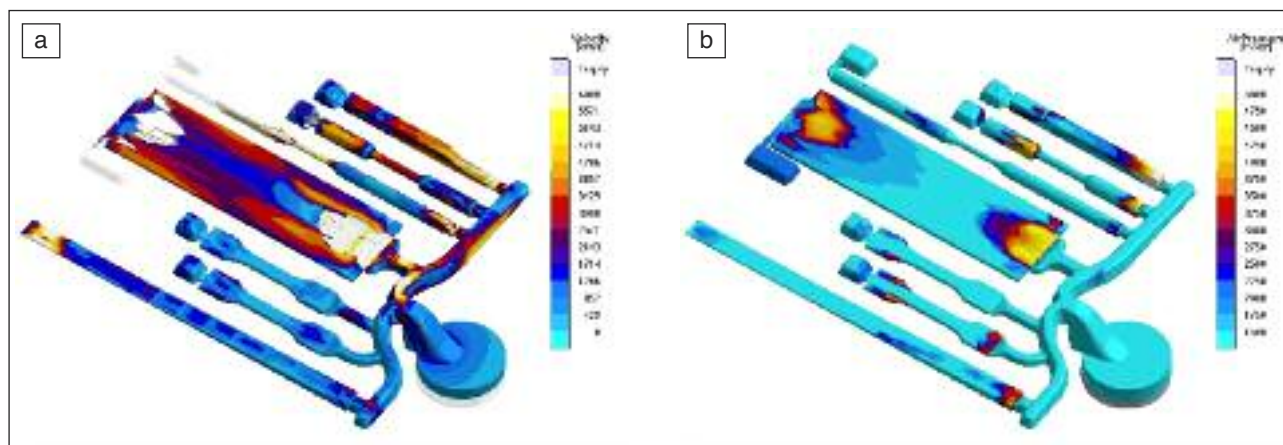
FIG. 13 *Calculated (a) melt velocity at 88% of die filling and (b) gas entrapment indicated by an air pressure criterion.*

(a) Velocità del metallo dopo l'88% di riempimento della cavità dello stampo e (b) zone di intrappolamento di gas indicate tramite l'ausilio del criterio Air pressure.

thickness of the specimens drawn from the plate. It is observed how the P_f is steady up to 0.119 wt.% Cr, even if the absolute value changes according to the analysed regions. Furthermore, the Cr addition to higher levels exerts a small impact on the P_f, with a reduction of about 4%. As evidenced from Figure 12, the displacement to fracture seems to suffer a loss mostly by an increased Cr content from 0.119 to 0.153 wt.%, with a general reduction of about 11%.

In general, fracture can of course be initiated both due to the presence of internal defects and due to the presence of surface defects. Internal defects are less likely to initiate fracture in plate bending tests. The low bending properties in the zones 1, 4 and 6 are ascribed to the presence of casting defects, previously revealed by X-ray investigations, which are mainly located in the central regions of the thickness of the tested specimens. It was beyond the scope of the present study to quantify the amount and the layer interested by casting defects, but it is known that these vary significantly throughout a HPDC component [46]. In addition, the large strain behaviour involves a strong interaction of plastic flow with eutectic silicon and Fe-rich intermetallic particles. The cracking of eutectic silicon and Fe-rich particles due to high tensile stresses induced by plastic deformation in the α-Al matrix significantly contribute to fracture. Cracked particles serve as nucleation sites for voids that eventually lead to fracture of the alloys [47]. In the present work, higher area fraction of intermetallic particles, especially sludge particles, act as weak regions, facilitating voids nucleation. Furthermore, by increasing the dimension and area fraction of brittle particles, the interparticle spacing of the particles generally reduce, providing easy pathways for macro cracks to propagate through them leading to fracture of the bulk material. This behaviour is more pronounced through the clustering phenomenon and the irregular distribution of secondary $\alpha\text{-Al}_x(\text{Fe,Mn,Cr})_y\text{Si}_z$ particles. Therefore, the fracture of sound specimens drawn from zones 2, 3 and 5 are preferentially ascribed to the increasing dimension and area fraction of brittle intermetallic compounds that form as the Cr level is increased.

In all the materials, general yielding takes place at a load of ~880 N, showing that the amount of the intermetallic phases has no influence on their yielding behaviour. The yield behaviour is largely determined by the relatively high supersaturation of atoms (Mg, Cu, Zn and Si) in α-Al matrix, which is referred to the high solidification rate. The Cr addition seems to not affect the yield point in the T1-condition, as well as seen in

the T6 temper where the globular α-Al(Fe,Mn,Cr)Si precipitates lead to the improvement of the ductility of material, more than a strengthening mechanism [11,16]. Using the equation given by Navier [48] it is possible to estimate the yield stress yd of the materials under study

$$\sigma_{yd} = \frac{M \cdot y}{I} = 142\,\text{MPa} \qquad (4)$$

where M is the bending moment, I the area moment of inertia of the cross section about the neutral axis and y is the distance of outermost fibres from the neutral axis. Previous results carried out by means of uniaxial tensile testing estimated yield stress, actually 0.2% proof stress, equal to 146 MPa [22]. As reported elsewhere [46], defects considerably influences the plastic properties of the material but not the elastic characteristics.

Numerical simulation results
The presence of defects in the diecast plates, evidenced by X-ray inspections, was studied by means of numerical simulation tools. From numerical simulation results it was possible to demonstrate how a good compromise between filling and decreasing melt temperature was obtained. Too slow die filling increases the risk of freezing by decreasing the melt temperature below the alloy-dependent coherence temperature. The calculated melt velocity at 88% of die filling is shown in Figure 13a, where the velocity distribution is mapped throughout the casting. It is observed how the liquid metal fill front progresses as nonplanar metal front in the die with a higher speed at the boundary of the plate (~35 ms^{-1}) and lower in the central part (~15 ms^{-1}). Metal fronts converge and surround pockets of air, resulting in entrapped gases in the far side of the plate.

The presence of defects was also investigated by an Air Pressure criterion, which represents the air pressure within a gas pocket enclosed in diecasting and it can suggest possible gas entrapment within the final casting [25]. The Air Pressure criterion revealed higher pressure values in the region close to the overflows of the plate (Figure 13b). This could confirm the highest porosity amount from the X-ray investigations.

CONCLUSIONS
The microstructure and bending properties of a high-pressure diecast AlSi9Cu3(Fe) has been investigated at various Cr contents. Based on the results obtained in the present study, the following conclusions can be drawn.
• Plates diecast from AlSi9Cu3(Fe) alloy with different Cr contents

present similar salient microstructural features, such as positive eutectic segregation bands, ESCs.

- The morphology of primary sludge compounds is mainly cubic-type, such as polyhedral, star-like and blocky. At 0.153 wt.% Cr content, sludge particles are found to show an exploded shape. The proeutectic α-Al$_x$(Fe,Mn,Cr)$_y$Si$_z$ intermetallics show blocky or polyhedral morphology at any Cr level.
- The area fraction of Fe-rich intermetallic compounds increases as the Cr content increases. Any increase in the area percentage of the particles is related to the size increase, which follows the three-parameter lognormal distribution. Contrary the morphology of the particles remains constant.
- At the holding temperature used for the different EN AC-46000 type alloys, sludge forms mainly during the transport of molten metal from the casting furnace to the shot sleeve and inside the cold chamber, the sludge can be formed at the wall and eventually separate before the melt entered the die cavity.
- Sludge segregates in the central region of the cross section of the plates with a mechanism similar to that suggested for the ESCs entrapment.
- The fracture load and, mostly, the displacement to fracture are sensitive to casting defects and Cr content; these values decrease in the defect regions of the diecast plate and even more for Cr level exceeding 0.12 wt.%. Contrary, casting defects and Cr addition seem to not affect the yielding behaviour of the alloy.
- Casting defects, such as gas entrapment, can be predicted with numerical simulation tools, by means of air pressure criterion.

REFERENCES

[1] European Aluminium Association (EAA) - Organisation of European Aluminium Refiners and Remelters, Aluminium Recycling in Europe - The Road to High Quality Products, 2004, pp. 1-52.

[2] http://recycling.world-aluminium.org

[3] U.M.J. Boin, M. Bertram, JOM 57 (2005) 26-33.

[4] Ch. Schmitz, Handbook of Aluminium Recycling, Vulkan-Verlag Gmbh, Essen, Germany, 2006

[5] S. Seifeddine, I.L. Svensson, Proc. Int. Conf. High Tech Die Casting, Montichiari, Italy, April 9-10, 2008, paper no. 15.

[6] S. Seifeddine, S. Johansson, I.L. Svensson, Mater. Sci. Eng. A 490 (2008) 385-390.

[7] G. Gustafsson, T. Thorvaldsson, G.L. Dunlop, Metall. Trans. A 17 (1986) 45-52.

[8] Z. Ma, A.M. Samuel, F.H. Samuel, H.W. Doty, S. Valtierra, Mater. Sci. Eng. A 490 (2008) 36-51.

[9] J.Y. Hwang, H.W. Doty, M.J. Kaufman, Mater. Sci. Eng. A 488 (2008) 496-504.

[10] S.G. Shabestari, M. Keshavarz, M.M. Hejazi, J. Alloys Compd. 477 (2009) 892-899.

[11] S. Murali, K.S. Raman, K.S.S. Murthy, Mater. Charact. 33 (1994) 99-112.

[12] D.A. Granger, R.R. Sawtell, M.M. Kersker, AFS Trans. 92 (1984) 579-586.

[13] P. Ashtari, H. Tezuka, T. Sato, Scripta Mater. 53 (2005) 937-942.

[14] Yen-Hung Tan, Sheng-Long Lee1, Yu-Lom Lin, Metall. Mat. Trans. A 26 (1995) 1195-1205.

[15] L.A. Narayanan, Crystallization and Dissolution studies of iron intermetallics in Al-Si alloys, PhD Thesis, McGill University, Montreal, Quebec, Canada, 1994.

[16] H.Y. Kim, S.W. Han, H.M. Lee, Mater. Lett. 60 (2006) 1880-1883.

[17] Witthaya Eidhed, J. Mater. Sci. Technol. 24 (2008) 45-47.

[18] L.F. Mondolfo, Aluminum Alloys: Structure and Properties, fist ed., Butterworths, London, 1976.

[19] M. Makhlouf, D. Apelian, Casting characteristics of aluminum die casting alloys, Report performed under DOE contract number DEFC07-99ID13716, (2002), 1-46.

[20] S.G. Shabestari, Mater. Sci. Eng. A 383 (2004) 289-298.

[21] S.G. Shabestari, J.E. Gruzleski, Metall. Mat. Trans. A 26 (1995) 999-1006.

[22] G. Timelli, F. Bonollo, Mater. Sci. Eng. A 528 (2010) 273-282.

[23] J.L. Jorstad, Die Cast. Eng. 11/12 (1986) 30-36.

[24] J. Gobrecht, Giesserei 61 (1975) 263-265.

[25] MAGMASOFT® v.4.4, 2006. MAGMAhpdc Module Manual, MAGMA Giessereitechnologie GmbH.

[26] H.I. Laukli, C.M. Gourlay, A.K. Dahle, O. Lohne, Mater. Sci. Eng. A 413-414 (2005) 92-97.

[27] C.M. Gourlay, H.I. Laukli, A.K. Dahle, Metall. Mater. Trans. A 38 (2007) 1833-1844.

[28] S. Otarawanna, C.M. Gourlay, H.I. Laukli, A.K. Dahle, Metall. Mater. Trans. A 40 (2009) 1645-1659.

[29] C.M. Gourlay, A.K. Dahle, Nature 445 (2007) 70-73.

[30] C.M. Gourlay, H.I. Laukli, A.K. Dahle, Metall. Mater. Trans. A 38 (2007) 1833-1844.

[31] S. Otarawanna, H.I. Laukli, C.M. Gourlay, A.K. Dahle, Metall. Mater. Trans. A 41 (2010) 1836-1846.

[32] G. Timelli, S. Ferraro, F. Grosselle, F. Bonollo, F. Voltazza, L. Capra, Metall. Ital. 103 (2011) 5-17.

[33] H.I. Laukli, A. Graciotti, O. Lohne, H. Gjestland, S. Sannes, NADCA Trans. 21 (2002) 1-4.

[34] M. Gershenzon, P.W. Rohan, M.T. Murray, Proc. 20th Int. Die Casting Congr. Expo., NADCA, Cleveland, OH, (1999), 305-315.

[35] H.I. Laukli, O. Lohne, S. Sannes, H. Gjestland, L. Arnberg, Int. J. Cast Met. Res. 16 (2003) 515-521.

[36] H.I. Laukli, C.M. Gourlay, A.K. Dahle, Metall. Mater. Trans. A 36 (2005) 805-818.

[37] F. Grosselle, G. Timelli, F. Bonollo, R. Molina, Metal. Sci. Technol. 27 (2009) 2-10.

[38] L.F. Mondolfo, Manganese in Aluminum Alloys, The Manganese Center, Paris, 1978.

[39] M. Warmuzeka, W. Ratuszekb, G. S k-sas, Mater. Charact. 54 (2005) 31-40.

[40] A.L. Dons, Z. Metallkd. 75 (1984) 170-174.

[41] M. Tiryakioglu, Mater. Sci. Eng. A 473 (2008) 1-6.

[42] M.R. Ghomashchi, J. Mater. Processing Technol. 52 (1995) 193-206.

[43] W. Sequeira, G. Dunlop, Die Cast. Eng. 48 (2004) 62-75.

[44] A. Flores, J. C. Escobedo, M. Mendez, J. Mendez, Proc. 16th Int. Die Casting Congr. Expo., Detroit, MI, (1991), 293-297.

[45] H.I. Laukli, High Pressure Die Casting of Aluminium and Magnesium Alloys - Grain Structure and Segregation Characteristics, PhD thesis, Norwegian University Of Science and Technology (NTNU), Trondheim, 2004.

[46] G. Timelli, Metal. Sci. Technol. 28 (2010) 9-17.

[47] L.L. Mishnaevsky Jr., N. Lippmann, S. Schmauder, P. Gumbsch, Eng. Fract. Mech. 63 (1999) 395-411.

[48] N.E. Dowling, Mechanical behaviour of materials, Second edition, Prentice Hall, Upper Saddle River, Ney Jersey, (1999), 152-153.

Abstract

Proprietà microstrutturali e caratteristiche a flessione di leghe di alluminio pressocolate al variare del contenuto di Cromo

Parole chiave:
alluminio e leghe, solidificazione, prove meccaniche, simulazione numerica,
riciclaggio, precipitazione, pressocolata, metallografia

Il riciclo dell'alluminio può condurre a risparmi energetici fino al 95% se confrontato con le tecnologie di produzione dell'alluminio primario, producendo il 99% in meno di emissioni inquinanti. Pertanto, l'alluminio secondario e le sue leghe stanno ottenendo ampi consensi in tutto il mondo e in svariati settori applicativi. La leggerezza dei prodotti in lega di alluminio contribuisce, inoltre, al risparmio di carburante e alla riduzione delle emissioni nel settore trasporti. Durante le operazioni di riciclaggio, la maggior parte dei componenti viene però mescolata, indipendentemente dalla composizione chimica, e durante le operazioni di rifusione dei rottami, si cerca di correggere la composizione finale della lega risultante direttamente in linea. Questa pratica, oltre a limitazioni economiche, presenta problematiche di natura chimico-metallurgica. Alcuni elementi chimici, come il Ferro, sono difficilmente rimovibili dal bagno liquido e quindi sempre presenti come impurezze nelle leghe commerciali. Diversi studi hanno dimostrato come la dimensione e la morfologia delle fasi infragilenti ricche in Fe possano essere alterate tramite l'aggiunta di Manganese e Cromo. In questo lavoro, le proprietà microstrutturali e le caratteristiche a flessione di una lega AlSi9Cu3(Fe) sono state studiate su delle piastre pressocolate al variare del tenore di Cr in lega (Figura 1).

I risultati ottenuti hanno dimostrato che tali piastre presentano sempre alcune caratteristiche microstrutturali salienti, come la presenza di bande di segregazione eutettica e cristalli pre-solidificati di alluminio (ESCs), indipendentemente dal tenore di Cr presente (Figure 4-6). L'incremento del livello di Cr in lega produce un aumento della quantità di cristalli primari di sludge, che generalmente si presentano in forma compatta (polyhedral, star-like e blocky), come mostrato in Figura 7, e solo nel caso dello 0.153 %pond di Cr con morfologia esplosa (Figura 8). La dimensione complessiva, così come il volume (Tabella 2), delle fasi intermetalliche ricche in Fe, $Al_x(Fe,Mn,Cr)_ySi_z$, cresce con l'incremento del livello di Cr secondo una distribuzione log-normale a tre parametri (Figura 10), mentre la morfologia delle particelle stesse rimane costante. I grossi cristalli primari di sludge, alla temperatura di mantenimento del bagno utilizzata nel presente lavoro (690 ± 5°C), si formano principalmente durante le operazioni di tazzaggio e all'interno della camera di iniezione, dove nucleano a ridosso delle pareti e vengono trasportate dal metallo liquido durante le fasi di iniezione. Tali particelle tendono a segregare verso il centro delle piastre con un meccanismo simile a quello degli ESCs.

Dal punto di vista meccanico, la caratterizzazione a flessione delle piastre ha evidenziato come il carico a rottura, ma soprattutto lo spostamento a rottura, sono sensibili al tenore di Cr in lega e alla presenza di difetti di colata; tali proprietà meccaniche diminuiscono sensibilmente in presenza di macrodifetti o con livelli di Cr superiori allo 0.12%pond (Figura 12). Al contrario, le proprietà elastiche sembrano non essere influenzate dalla presenza di difetti né dal tenore di Cr.

La presenza di difetti di colata, ascrivibili a porosità da gas (Figura 11), è messa in evidenza con l'ausilio della simulazione numerica di processo tramite il criterio dell'Air pressure (Figura 13).